euspen's 19th International Conference & Exhibition, Bilbao, ES, June 2019
www.euspen.eu

Theoretical analysis and experimental verification on the pneumatic hammer in aerostatic thrust bearings with porous restrictor

Hailong Cui*, Dajiang Lei, Lichao Guan, Xinjiang Zhang, Huan Xia

Institute of Machinery Manufacturing Technology, China Academy of Engineering Physics, Mianyang, 621000 People's Republic of China

cuihailong61@foxmail.com

Abstract
In this study, the computational fluid dynamics (CFD) method combined with dynamic meshing technology (DMT) were applied to calculate the dynamic stiffness and damping coefficient of aerostatic porous thrust bearings. The dynamic response of bearing system was obtained by solving the motion differential equation. The influences of permeability parameters and operating conditions on pneumatic hammer instability in aerostatic porous thrust bearings were also conducted both theoretically and experimentally. The difference between the calculation results and experimental data for both porous permeability of 1e-12 m^2 and 1e-13 m^2 are less than 5 %, which demonstrates that the pneumatic hammer of aerostatic porous bearing can be accurately predicted by the numerical model proposed in this study. The supply pressure and porous permeability should be reasonably controlled to avoid the occurrence of pneumatic hammer.

aerostatic bearings; porous restrictor; pneumatic hammer; dynamic meshing technology

1. Introduction

Due to the benefits of high running accuracy, low friction, long working life, aerostatic bearings have been successfully applied in the optical lithography, high-vacuum compatible condition, ultra-precision machining tool and positioning table. In recent years, researchers have been committed to improving the static and dynamic properties of aerostatic bearings by optimizing the geometric parameters and working conditions. However, the pneumatic hammer still appeared at certain conditions, which significantly reduced the stability of aerostatic bearings. Unfortunately, the methods for improving the load capacity and stiffness of aerostatic bearing may be induced the pneumatic hammer, such as the rise of supply pressure. Until now, the contradictory relationship between bearing stability and stiffness has not been effectively solved.

The reported literatures show that the study of pneumatic hammer was almost totally focused on aerostatic bearings with orifice restrictor, there were very few reports concentrated on pneumatic hammer in aerostatic porous bearings. Sneck [1] pointed out aerostatic porous thrust bearings had a relative narrow stable region. Sun [2] carried out a linear analysis on aerostatic porous thrust bearing, and concluded that bearing stability performance was determined by the gas compressibility, bearing mass, and viscous resistance of porous restrictor. Yoshimoto et al. [3] showed that the bearing stiffness can be improved by reducing the permeability of porous restrictor, but the lower the porous permeability, the more prone to pneumatic hammer. The above conclusions and results provide an effective reference for investigating the pneumatic hammer instability in aerostatic thrust bearings with porous restrictor. However, based on the previous results [4-5], the bearing dynamic stiffness and damping coefficient were strongly related to perturbation frequency, which was ignored in the existed numerical method for pneumatic hammer analysis. The existed literatures reveal that the relationship between pneumatic hammer instability in aerostatic porous thrust bearings and permeability parameters, operating conditions is not fully understood, which prohibits the widespread application of aerostatic porous bearings.

In this study, the computational fluid dynamics (CFD) method combined with dynamic meshing technology (DMT) were applied to calculate the dynamic stiffness and damping coefficient of aerostatic porous thrust bearings. The dynamic response of bearing system was obtained by solving the motion differential equation. The influences of permeability parameters and operating conditions on pneumatic hammer instability in aerostatic porous thrust bearings were also conducted both theoretically and experimentally.

2. Theoretical modeling

Geometric structure of aerostatic circular thrust bearings with porous restrictors is shown Fig.1. Compressed gas supplied by the feeding hole, flows through porous restrictor into bearing film, which was applied to support the bearing shaft. The gas motion in bearing film satisfies the following equations

$$\frac{\partial \rho}{\partial t} + div(\rho \vec{u}) = 0 \tag{1}$$

$$\begin{cases} \dfrac{\partial(\rho u)}{\partial t} + div(\rho \vec{u} u) = -\dfrac{\partial p}{\partial x} + \dfrac{\partial \tau_{xx}}{\partial x} + \dfrac{\partial \tau_{yx}}{\partial y} + \dfrac{\partial \tau_{zx}}{\partial z} + F_x \\ \dfrac{\partial(\rho v)}{\partial t} + div(\rho \vec{u} v) = -\dfrac{\partial p}{\partial y} + \dfrac{\partial \tau_{xy}}{\partial x} + \dfrac{\partial \tau_{yy}}{\partial y} + \dfrac{\partial \tau_{zy}}{\partial z} + F_y \\ \dfrac{\partial(\rho w)}{\partial t} + div(\rho \vec{u} w) = -\dfrac{\partial p}{\partial z} + \dfrac{\partial \tau_{xz}}{\partial x} + \dfrac{\partial \tau_{yz}}{\partial y} + \dfrac{\partial \tau_{zz}}{\partial z} + F_z \end{cases} \tag{2}$$

$$\frac{\partial(\rho T)}{\partial t} + div(\rho \vec{u} T) = div(\frac{k}{c_p} gradT) + S_T \tag{3}$$

And the pressure drop through porous restrictor can be expressed as

$$\nabla p_i = -\left(\sum_{j=1}^{3} D_{ij} \eta u_j + \sum_{j=1}^{3} C_{ij} \frac{1}{2} \rho |u| u_j \right) \quad (4)$$

Under steady-state condition, the pressure distribution of bearing film can be obtained by solving Eq. (1) to Eq. (4) based on the ANSYS Fluent software. And the static film force can be calculated by integrating the film pressure distribution.

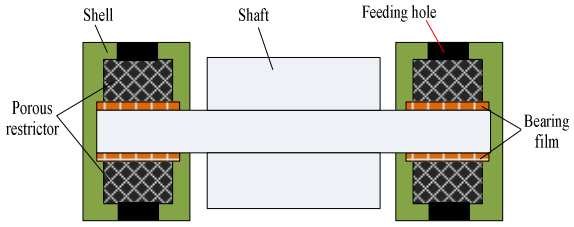

Fig. 1. Schematic of aerostatic circular thrust bearings with porous restrictors

In this study, the DMT in the ANSYS Fluent software was applied to calculate the dynamic film force. In the transient calculation, the moving boundary and mesh satisfies the following equations

$$\frac{d}{dt}\int_V \rho\phi dV + \int_{\partial V} \rho\phi\left(\vec{u} - \vec{u}_g\right)\cdot d\vec{A} = \int_{\partial V} \Gamma \nabla\phi \cdot d\vec{A} + \int_V S_\phi dV \quad (5)$$

$$\frac{d}{dt}\int_V \rho\phi dV = \frac{\left(\rho\phi V\right)^{n+1} - \left(\rho\phi V\right)^n}{\Delta t} \quad (6)$$

$$V^{n+1} = V^n + \frac{dV}{dt}\Delta t \quad (7)$$

$$\frac{dV}{dt} = \int_{\partial V} \vec{u}_g \cdot d\vec{A} = \sum_j^{n_f} \vec{u}_{g,j} \cdot \vec{A}_j \quad (8)$$

$$\vec{u}_{g,j} \cdot \vec{A}_j = \frac{\delta V_j}{\Delta t} \quad (9)$$

The dynamic film force can be obtained based on Eq. (1) to Eq. (9), at the given small amplitude periodic incentive with a certain frequency, the bearing film complex stiffness can be denoted as

$$K^* = \frac{\Delta F}{\Delta h} \quad (10)$$

where is the dynamic film force, is the periodic incentive and can be denoted as

$$\Delta h = A e^{i\omega t} \quad (11)$$

The film dynamic stiffness and damping coefficient at a certain frequency can be expressed by the following equations

$$K = \mathrm{Re}(K^*) \quad (12)$$

$$C = \mathrm{Im}(K^*) \quad (13)$$

The dynamic response of bearing system satisfies the following expression

$$M\ddot{x} + C(\omega)\dot{x} + K(\omega)x = F(t) \quad (14)$$

The detail computational conditions and input parameters of the numerical calculation are listed in Tab. 1

Tab. 1 The detail computational conditions and input parameters

Calculation conditions and input parameters	Value
Solver	Absolute transient pressure-based
Solution method	SIMPLEC
Solution initialization	Standard initialization
Viscous	Laminar
Gas	Ideal-gas
Dynamic viscosity	1.789e-5 Kg/(m•s)
Temperature	293 K
Specific heat	1006.43 J/(kg•K)
Thermal conductivity	0.0242 W/(m•K)
Operating(Atmospheric) pressure	101325 Pa
Inlet(Gauge) pressure	4 to 7 bar
Outlet(Gauge) pressure	1 bar
Film thickness	10 μm
Thrust bearing outer diameter	80 mm
Thrust bearing inner diameter	56 mm
Thrust porous restrictor outer diameter	80 mm
Thrust porous restrictor outer diameter	56 mm
Porosity	0.18
Porous permeability	1e-11 to 1e-15 m^2

3. Results and Discussions

3.1. Effect of supply pressure on the pneumatic hammer

At the system incentive of $F(t) = \sin\left(4\times10^3 \pi t\right)$ and the porous permeability of 1e-13 m^2, the effect of supply pressure on the pneumatic hammer is shown in Fig.2. It can be observed from Fig.2 that the system response increases with a growth of supply pressure. At the range of supply pressure from 0.4 MPa to 0.6 MPa, the bearing system is still in stable state. At the critical supply pressure of 0.64 MPa, the bearing system is in the critical stable state. At the supply pressure more than 0.64 MPa, the bearing system is in an unstable state. It can be seen from Fig.2 that the pneumatic hammer appears at the supply pressure of 0.7 MPa. The pneumatic hammer destroys the stability of the bearing support, cause the gas film lubricating layer to fail, and damage the bearing surfaces. Therefore, the supply pressure should be reasonably controlled to avoid the occurrence of pneumatic hammer.

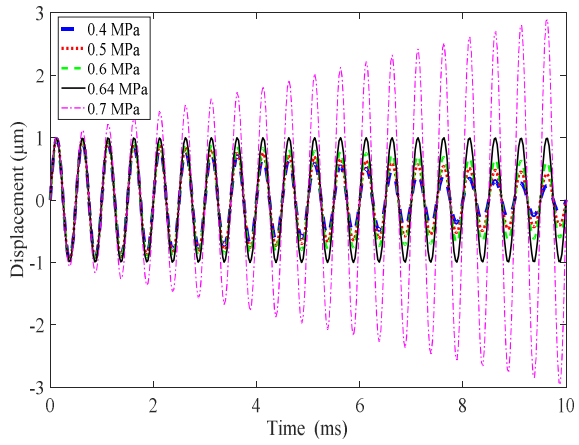

Fig. 2. Effect of supply pressure on the pneumatic hammer

3.2. Effect of porous permeability

At the system incentive of $F(t)=\sin\left(4\times10^{3}\pi t\right)$ and the supply pressure of 0.6 MPa, the effect of porous permeability on the pneumatic hammer is shown in Fig.3. It can be obtained from Fig. 3 that the response of bearing system is significantly influenced by the permeability of porous materials. The response of bearing system increases with a rise of porous permeability. At the porous permeability less than 1e-13 m^2 , the bearing system is still in stable state. The pneumatic hammer appears at the porous permeability more than 1e-12 m^2. Therefore, the porous permeability should be reasonably controlled to avoid the occurrence of pneumatic hammer.

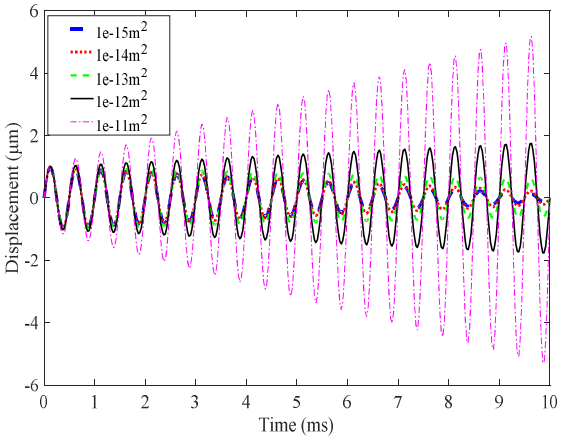

Fig. 3. Effect of porous permeability on the pneumatic hammer

3.3. Effect of porous permeability

The experiment platform for measuring the pneumatic hammer of aerostatic thrust bearings is constructed in this study, as shown in Fig.4. The experiment platform is mainly comprised by the following parts: aerostatic porous bearings, control system and results display, vibration isolating system, pressure regulating valve and pressure sensor, acceleration sensor. protective shield and measuring platform.

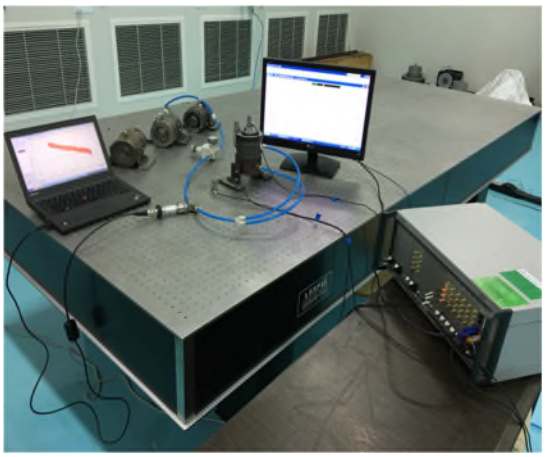

(a) Experiment platform

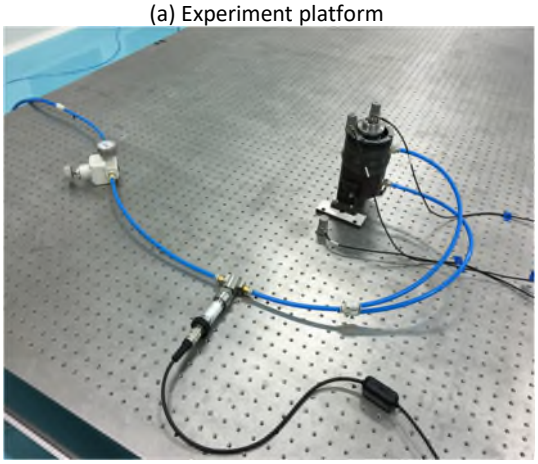

(b) Aerostatic porous bearings

Fig. 4. Experiments on the pneumatic hammer

At the porous permeability of 1e-12 m^2 and 1e-13 m^2, the critical supply pressure corresponding to the pneumatic hammer is shown in Tab. 2. It can be obtained from Tab.2 that the difference between the calculation results and experimental data for both porous permeability of 1e-12 m^2 and 1e-13 m^2 are less than 5 %, which demonstrates that the pneumatic hammer of aerostatic porous bearing can be accurately predicted by the numerical model proposed in this study.

Tab.2 Results of numerical calculations and experimental tests

Porous permeability	Calculation results (MPa)	Experimental data(MPa)	Difference
1e-12 m^2	0.53	0.508	4.2 %
1e-13 m^2	0.64	0.616	3.9 %

4. Conclusions

In this study, the computational fluid dynamics (CFD) method combined with dynamic meshing technology (DMT) were applied to calculate the dynamic stiffness and damping coefficient of aerostatic porous thrust bearings. The dynamic response of bearing system was obtained by solving the motion differential equation. The influences of permeability parameters and operating conditions on pneumatic hammer instability in aerostatic porous thrust bearings were also conducted both theoretically and experimentally.

At the range of supply pressure from 0.4 MPa to 0.6 MPa, the bearing system is still in stable state. At the critical supply pressure of 0.64 MPa, the bearing system is in the critical stable state. At the supply pressure more than 0.64 MPa, the

bearing system is in an unstable state. At the porous permeability less than 1e-13 m^2, the bearing system is still in stable state. The pneumatic hammer appears at the porous permeability more than 1e-12 m^2. The difference between the calculation results and experimental data for both porous permeability of 1e-12 m^2 and 1e-13 m^2 are less than 5 %, which demonstrates that the pneumatic hammer of aerostatic porous bearing can be accurately predicted by the numerical model proposed in this study.

References

[1] SNECK H J 1968 *J. Lub. Technol.* 804-09
[2] SUN D C 1973 *J. Lub. Technol.* 457-68
[3] Yoshimoto S and Kohno K 2001 *J. Tribol.* **123** 501-08
[4] Chen X D, Zhu J C, and Chen H 2013 *Adv. Manuf.* **1** 82-86
[5] Yu P L, Chen X D, Wang X L, and Jiang W 2015 *Int. J. Precis. Eng. Man.* **16** 1771-77